PAPER

Performance Evaluation and Link Budget Analysis on Dual-Mode Communication System in Body Area Networks

Jingjing SHI[†a)], ***Member***, **Yuki TAKAGI**[†], ***Nonmember***, **Daisuke ANZAI**[†b)], ***Member***, ***and*** **Jianqing WANG**[†c)], ***Fellow***

SUMMARY Wireless body area networks (BANs) are attracting great attention as a future technology of wireless networks for healthcare and medical applications. Wireless BANs can generally be divided into two categories, i.e., wearable BANs and implant BANs. However, the performance requirements and channel propagation characteristics of these two kinds of BANs are quite different from each other, that is, wireless signals are approximately transmitted along the human body as a surface wave in wearable BANs, on the other hand, the signals are transmitted through the human tissues in implant BANs. As an effective solution for this problem, this paper first introduces a dual-mode communication system, which is composed of transmitters for in-body and on-body communications and a receiver for both communications. Then, we evaluate the bit error rate (BER) performance of the dual-mode communication system via computer simulations based on realistic channel models, which can reasonably represent the propagation characteristics of on-body and in-body communications. Finally, we conduct a link budget analysis based on the derived BER performances and discuss the link parameters including system margin, maximum link distance, data rate and required transmit power. Our computer simulation results and analysis results demonstrate the feasibility of the dual-mode communication system in wireless BANs.

key words: *body area networks, dual-mode communication system, bit error rate, link budget*

1. Introduction

Wireless body area networks (BANs) are attracting great attention in the field of healthcare and medical applications. Wireless BANs are generally divided into two groups, such as wearable BANs and implant BANs according to their locations on or in the human body where they operate [1]. Wearable BANs are mainly used to monitor a person's health condition in order to decrease the loads of doctors and nurses [2]. Implant BANs can be used to monitor the vital signals inside the human body. One of the typical applications is wireless monitoring of the cardiac pacemaker data in order to always keep an adequate pulse rate for cardiac disease patients. Moreover, medical examination such as wireless capsule endoscopy is also a promising application [3], [4]. A wireless capsule endoscope contains color camera, light source, and battery and is used by swallowing to transmit images to the outside receiver for the purpose of assisting in diagnosing gastrointestinal conditions.

Manuscript received October 22, 2013.
Manuscript revised January 29, 2014.

[†]The authors are with the Graduate School of Engineering, Nagoya Institute of Technology, Nagoya-shi, 466-8555 Japan.
a) E-mail: shi@nitech.ac.jp
b) E-mail: anzai@nitech.ac.jp
c) E-mail: wang@nitech.ac.jp

DOI: 10.1587/transcom.E97.B.1175

In both wearable BANs and implant BANs, such healthcare and medical applications require reliable wireless communication channel, reasonable data rates for real-time transmission, and extremely low power consumption for increased device longevity [5]. Bluetooth and Zigbee are candidates for the communication schemes that can be applied. However, Bluetooth supports no more than seven sensors per piconet, so it may restrict network extendability. Furthermore, when assuming a healthcare and medical application, various transmission speeds are required. For example, a blood sugar sensor requires 0.1 kbps at most, while a wireless capsule endoscope application requires 1 Mbps at least [6]. In other words, the wearable BANs accept low data rates, but the implant BANs may require high data rates to transmit capsule endoscope video images in real-time. From these reasons, the feature is difficult to satisfy by Bluetooth and Zigbee.

Furthermore, the propagation characteristics of wearable BANs and implant BANs are quite different from each other. This is because wireless signals of wearable BANs are transmitted along the human body surface approximately, whereas the signals of implant BANs are transmitted through the various kinds of human tissues. Several studies have been performed to characterize the two propagation channels for wearable and implant BANs [7]–[10], which demonstrated a significant frequency dependence for both on-body and in-body path loss. The lower the frequency is, the smaller the path loss is. Consequently, we should individually optimize the transmission schemes for on-body and in-body communications because of the difference of the channel characteristics. In this paper, for the purpose of solving the optimization problem for the transmission schemes in wearable and implant BANs, we develop a dual-mode communication structure. For on-body communication, high date rates are not necessary. Carrier signal frequencies below dozens of ten MHz are therefore good candidates because the human body acts as a transmission medium in this frequency band [11]. While for in-body communication, it is more desirable for the transmitter to have a relative high date rate in order to satisfy the requirement of image transmission. Moreover, the miniaturization of the transmit antenna for implantation inside the human body is essential. We have previously proposed for in-body communications by using extremely short pulses at GHz, i.e., 3.4–4.8 GHz, defined as UWB low band signals, because of its superior advantages on very high data rates

for real-time transmission [12]. However, the pulses suffer from severe attenuations through the human tissues and this problem makes it difficult to be received by only the out-body receiver. A diversity technique has to be employed to solve this problem, it increases the complexity of the receiver structure. As a result, for the practical use in the implant BAN applications, a carrier signal at several hundreds of MHz may be more suitable to provide a better communication performance and a relative high-speed transmission. This is because the signal at this frequency band is relatively less attenuated, and small antennas for implantation are also easier to achieve compared to that at dozens of ten MHz. Therefore, in accordance with the different requirements, we consider different architectures for the on-body and in-body transmitters. Besides, we investigate the BER performance of the dual-mode communication system via computer simulations based on realistic channel models, which can well represent the propagation characteristics of on-body and in-body communications. Finally, we perform a link budget analysis based on derived BER performance and discuss the link parameters including system margin, maximum link distance, data rate and transmit power. Our computer simulation and analysis results demonstrate the feasibility of the dual-mode communication system in wireless BANs.

The remaining of this paper is organized as follows. Section 2 presents the dual-mode communication structure for the in-body and on-body communications. Section 3 describes channel models of the in-body and on-body communications. Then Sect. 4 demonstrates and discusses the bit error rate (BER) performances by the computer simulations, and Sect. 5 discusses the link budget parameters to clarify the feasibility of dual-mode communication system. Finally, Sect. 6 concludes this paper.

2. Dual-Mode Communication System

2.1 Overview of Dual-Mode Communication System

Figure 1 shows the overview of the dual-mode communication system developed in this paper. There are two kinds of transmitters in Fig. 1, namely, one is an on-body transmitter located on the human body surface, and the other one is an in-body transmitter located inside of the human body [13]. On the other hand, as can be seen in Fig. 1, there is only one dual-mode receiver on the surface of human body. That is to say, in this dual-mode communication system, the receiver can receive both the signals from the in-body and on-body transmitters and gather all the vital data over the whole human body. As previously introduced BAN requirements, that is, the wearable BAN application needs low data rates while the implant BAN application may demand high data rates, this study decides to choose human body communication (HBC) band at 30 MHz as the carrier frequency of the on-body transmitter and medical implant communication service (MICS) band at 400 MHz as the carrier frequency of the in-body transmitter, respectively. It should be noted that these adopted frequency bands are suggested by IEEE 802.15.6 standard [14], which has been released in Feb. 2012 for medical BANs standardization.

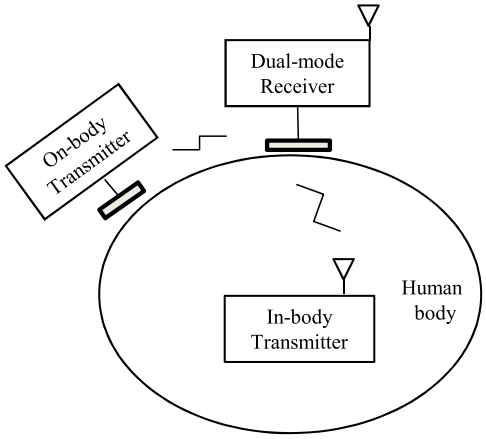

Fig. 1 Overview of dual-mode communication system.

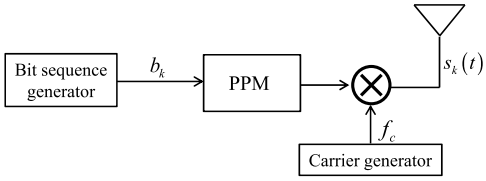

Fig. 2 Transmitter structure.

2.2 Transmitter

The structure of the transmitter is shown in Fig. 2. The bit sequence generator in Fig. 2 generates information bit sequence $b_1, b_2, \cdots, b_k, \cdots, b_K$, where b_k represents the k-th bit information ($b_k \in \{0, 1\}$). The information bit b_k is sent by using pulse position modulation (PPM) scheme. The PPM scheme transmits the bit information as a pulse location. The k-th transmit signal $s_k(t)$ can be expressed as

$$s_k(t) = \cos\left[2\pi f_c(t - b_k T_c - kT_s)\right] \tag{1}$$

where f_c, T_s and T_c indicate the carrier frequency, symbol duration and signal duration, respectively. In the case of binary PPM, T_c can be calculated as $T_s/2$. Figure 3 shows an example of the transmitted PPM signals. Note that the carrier frequencies of the on-body and in-body transmitters are set to different frequencies.

2.3 Receiver

The structure of the receiver is shown in Fig. 4. Since the on-body and in-body transmitters use the different carrier frequencies, the dual-mode receiver has two types of bandpass filters (BPFs) working at the carrier frequencies plus/minus twice data rate f_b ($=1/T_s$) of the on-body and in-body transmitters, respectively. Both of the bandpass filters are based on Nyquist cosine roll-off filters, so they can be expressed as

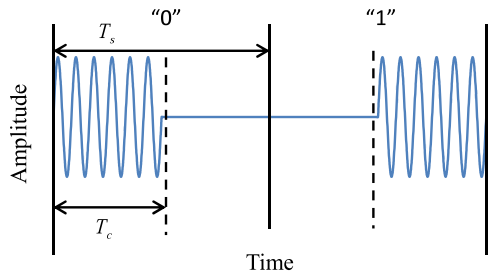

Fig. 3 An example of transmitted PPM signals.

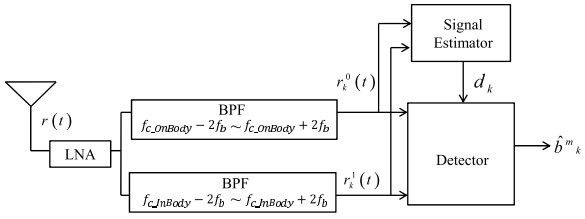

Fig. 4 Receiver structure.

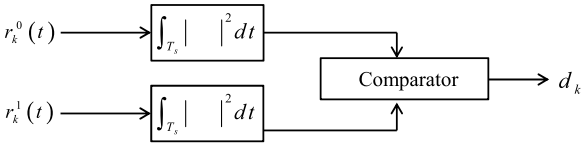

Fig. 5 Signal estimator structure.

$$h_{roll-off}(t) = f_s \frac{\sin(\pi f_s t)}{(\pi f_s t)} \frac{\cos(\alpha\pi f_s t)}{1-(2\alpha f_s t)^2} \tag{2}$$

where α is a roll-off rate. Here, f_s is calculated from the bandwidth B of the bandpass filter, which is given by

$$B = \frac{(1+\alpha)f_s}{2}. \tag{3}$$

Before demodulating the received signals, at first, we estimate which transmitter sends the signals. Figure 5 shows the signal estimator structure. The signal estimator calculates the energies of the filtered signals $r_k^0(t)$ and $r_k^1(t)$ in the integration interval of T_s. $r_k^0(t)$ denotes the on-body received signal, and $r_k^1(t)$ denotes the in-body received signal. They are the corresponding signals after the on-body mode and in-body mode band pass filters, respectively. The outputs of the integrators E_{on} and E_{in} can be expressed as

$$E_{on} = \int_0^{T_s} [r_k^0(t)]^2 dt \tag{4}$$

$$E_{in} = \int_0^{T_s} [r_k^1(t)]^2 dt \tag{5}$$

where E_{on} and E_{in} denote the energies of the received signals from the on-body and in-body transmitters, respectively. Comparing E_{on} and E_{in}, we estimate the signal estimator output as

$$d_k = \begin{cases} 0 & \text{if } E_{on} > E_{in} \\ 1 & \text{otherwise} \end{cases} \tag{6}$$

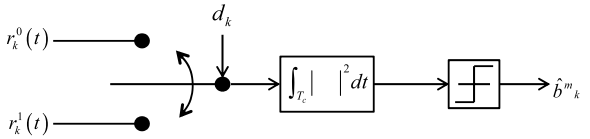

Fig. 6 Detector structure.

where $d_k = 0$ and $d_k = 1$ indicate that the received signals come from the on-body and in-body transmitter respectively.

Next, we decide the received information bit by using d_k, $r_k^0(t)$, and $r_k^1(t)$. The structure of the detector is shown in Fig. 6. As for detection of the received signals, we employ an energy detection scheme in this study. Based on the signal estimator output d_k, the detector selects $r_k^0(t)$ or $r_k^1(t)$. The energy of the selected signal r_k^m $(m = 0, 1)$ is detected in two kinds of integration time as

$$E_k^m = \int_0^{T_c} [r_k^m(t)]^2 dt \tag{7}$$

$$\overline{E}_k^m = \int_{T_c}^{T_s} [r_k^m(t)]^2 dt. \tag{8}$$

Comparing E_k^m and $\overline{E}_k^m$, the k-th information bit $\hat{b}_k^m$ can be determined as follows:

$$\hat{b}_k^m = \begin{cases} 0 & \text{if } E_k^m > \overline{E}_k^m \\ 1 & \text{otherwise.} \end{cases} \tag{9}$$

3. Channel Models

To evaluate the communication performance of the dual-mode transceivers, in addition to an additive white Gaussian noise (AWGN) channel model, this paper also considers realistic channel models, which were derived from anatomical human body models and reasonably represent the propagation characteristics of on-body and in-body communications.

Defining the transmitted and received signals as $s(t)$ and $r(t)$, respectively, $r(t)$ is given by

$$r(t) = h(t) \otimes s(t) + n(t) \tag{10}$$

In Eq. (10), $h(t)$ and $n(t)$ denote the impulse response of the on-body channel or in-body channel and the additive Gaussian noise at the receiver, respectively, and $\otimes$ denotes the convolution. The signals are transmitted along or through the human body so that the amplitude of the impulse response $|h(t)|$ is affected by shadow fading of the human body. In the channel modeling, we pay the attention to path losses in view of the receiver structure. We incorporated an anatomical Japanese male model with finite-difference time-domain (FDTD) numerical simulations to derive the on-body and in-body path loss characteristics. The employed Japanese male model consists of 51 types of biological tissue with 1.73 m tall and 65 kg weight. It was developed by National Institute of Information and Communication Technology, Japan. For deriving the on-body channel path loss

Table 1 Parameters for on-body and in-body path loss models.

	On-body model	In-body model
PL_0	35.4 dB	49.7 dB
n	1.8	5.5
d_0	10 cm	5 cm
σ	2.7 dB	8.2 dB

characteristics, a receiving electrode was placed in a typical use position in front of the belly, while the transmitting electrode was set at more than 30 locations on the body surface. On the other hand, in the in-body channel path loss calculations, a small dipole receiving antenna was placed at the same position as that in the on-body case in front of the belly, and the other small dipole antenna was arranged to take 30 locations inside the human body with three different polarizations. As a FDTD simulation result, both the on-body and in-body path loss were approximated as

$$PL_{dB} = PL_{0,dB} + 10n \log_{10}(d/d_0) + S_{dB} \tag{11}$$

where $PL_{0,dB}$ is the reference path loss at distance d_0, n is the path loss exponent, d indicates the distance between the transmitting antenna and receiving antenna, and S denotes the path loss variation from its average value, i.e., the shadow fading.

The FDTD-derived parameters of on-body and in-body path loss channel models are tabulated in Table 1 [12], [15], which have been examined by experiments in actual human bodies for on-body channel and tissue-equivalent liquid phantom for in-body channel. The shadow fading has been found to follow log-normal distribution in both the on-body channel and in-body channel. The corresponding parameter σ in the log-normal distribution was found to be about 2.7 dB for on-body channel and 8.2 dB for in-body channel. This also means that the on-body and in-body channel models are quite different from each other.

Moreover, since the shadow fading follows log-normal distribution, the received signal power P_r or the energy per bit E_b is also the same distribution. For a fixed noise power spectral density N_0 at the receiver, E_b/N_0 should exhibit the same statistical characteristic and is therefore also log-normal distributed, i.e., its probability density function (PDF) can be written as

$$p(E_b/N_0) = \frac{1}{\sqrt{2\pi}\sigma E_b/N_0} \exp\left(-\frac{(\ln[E_b/N_0]-\mu)^2}{2\sigma^2}\right) \tag{12}$$

where μ and σ are the statistical parameters in the log-normal distribution, and σ is equal to that given in Table 1.

4. Performance Evaluation

4.1 Setup of Computer Simulations

We conducted computer simulations with the above-described realistic on-body and in-body channel model parameters in order to evaluate the communication performances of the dual-mode transceivers. In the computer simulations, both of transmitters sent 100,000 bits at each E_b/N_0. We at first determined the energy for each bit as $E_b = 1$ Joule. Then we can obtain the N_0 when changing the E_b/N_0 at different values, for example, from 0 dB to 20 dB or 40 dB. At last, the BER was calculated by comparing the transmitted bit sequence and the received bit sequence. It should be emphasized that for the symbol timing and sampling clock synchronization, we assumed it perfectly performed with a proper length of pilot signals. The parameters of the computer simulation are summarized in Table 2. The data rates were set at the maximum permissible one in MICS 400 MHz band.

Table 2 Specifications for computer simulation.

Carrier frequency of on-body transmitter	30 MHz
Carrier frequency of in-body transmitter	400 MHz
Modulation scheme	PPM
Bit rate	0.3 Mbps
Symbol duration	3.3 μsec
Receiver structure	Energy detection
Roll-off rate α	0.5
Forward error correction	None

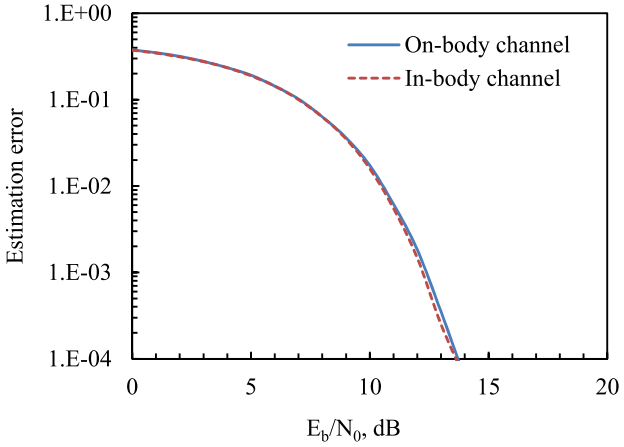

Fig. 7 Estimation error performance in AWGN channel.

4.2 Computer Simulation Results

Figures 7 and 8 show the E_b/N_0 against the estimation error performances of the signal estimator shown in Fig. 5 in the AWGN and shadow fading channels, respectively. As can be seen from these figures, because the estimation error performances are affected by the shadow fading channels, the corresponding performances become worse than those in the AWGN channels. Moreover, from Fig. 8, the performance of the in-body channel is evidently worse than that in the on-body channel. This is because the variance of the log-normal distribution parameter σ in the in-body channel is much larger than that in the on-body channel, which indicates the signals transmitted through the in-body channel suffer from larger shadow fading effect.

Figures 9 and 10 show the E_b/N_0 versus the BER performances in AWGN and shadow fading channels, respec-

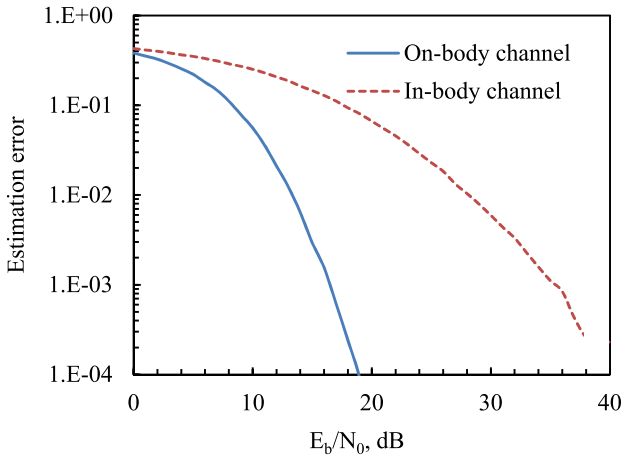

Fig. 8 Estimation error performance in shadow fading channel.

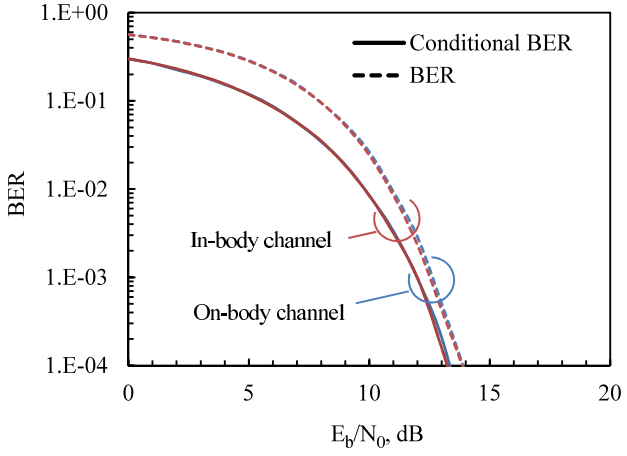

Fig. 9 BER performance in AWGN channel.

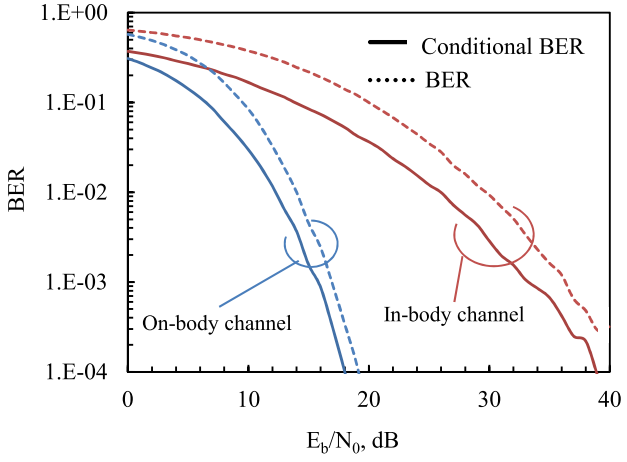

Fig. 10 BER performance in shadow fading channel.

tively. The solid lines plotted in these two results indicate the calculated conditional BER performances without considering the estimation error in the signal estimator in Fig. 4. In other words, they represent the BER performances when assuming the signal estimation process is perfect. By contrast, the dotted lines indicate the BER performances with the consideration of the error of signal estimation in Fig. 4. It can be seen in Fig. 9 that on-body and in-body BER curves are almost overlapped in AWGN channel. Meanwhile, it can also be observed from these figures that the tendency of the BER performance is almost the same as that of the signal estimation performance. Compared to the conditional BER performances, the BER performances show somewhat worse results because of the signal estimation error. However, these performance degradations of the E_b/N_0 in the shadow fading channel are only several dB. For example, in Fig. 10, the E_b/N_0 in the conditional BER performance is around 13 dB and 27 dB at BER = 10^{-2} in on-body and in-body channels, respectively, but the performance deteriorations between the conditional BER and BER were observed to range from only 1 to 3 dB. This suggests that a good on-body communication performance may be easily achieved at a low transmit power level, but the in-body communication may be significantly affected by the shadow fading effect of various different tissues.

5. Link Budget Analysis

5.1 Link Budget Parameters

A link budget in the case of our dual-mode system is the accounting of all of the gains and losses from the on-body and in-body transmitters, through the transmission medium, i.e., human body tissues to the dual-mode receiver. The on-body transmission corresponds to on-body to on-body link, while the in-body to on-body transmission corresponds to in-body to on-body link. They account for the attenuations of the transmitted signals due to the on-body and in-body channel propagation, as well as the antenna gains, feedline and miscellaneous losses [16]. In order to analyze the link budget in the on-body and in-body channels, besides the derived path loss, the noise characteristics and the possible transmitted signal power also have to be calculated. First, let us determine the noise characteristics at the receiver. To simplify the noise situation, we assume a single equivalent noise source as AWGN. This noise is typically thermal and introduced by the receive antenna and the front-end circuit of the receiver. The thermal noise power spectrum density (PSD) expressed in W/Hz is given by

$$N_0 = kT_a + k(N_F - 1)T_0 \tag{13}$$

where T_a is the receiving antenna temperature, $T_0 = 300$ K is the environment temperature, $k = 1.38 \times 10^{-23}$ J/K is the Boltzmann constant, and finally N_F is the noise figure of the receiver front-end. Since the receiver is mounted on the surface of human body, a reasonable hypothesis is introduced that $T_a = T_0 = 300$ K. Equation (13) can therefore be rewritten in decibel as

$$N_{0,dB} = 10\log_{10}(kT_0) + N_{F,dB} = -198\,\text{dBW/Hz}. \tag{14}$$

Secondly, for the on-body HBC band and in-body

MICS band transmission, we should first prescribe the maximum transmit power. For HBC band signals, there is not a common regulation. In Japan, a transceiver in this frequency band may be classified as extremely low power radio equipment in which the radiated electric field from the transceiver is requested not to exceed 500 μV/m or 54 dBμV/m at a distance of 3 m. If this requirement is met no license is needed for the transceiver. Thus, an HBC-based on-body communication link can be established under the extremely low power radio regulation. In fact, we have developed a HBC transmitter. The measured electric field strength at a distance of 3 m is lower than 30 dBμV/m when the transmit power is −20 dBm. Even if we use the transmit power as −10 dBm, the detected electric field strength would never exceed 50 dBμV/m, still satisfying the regulation of extremely low power radio station. As a result, we here use this power level in the on-body link budget analysis. On the other hand, according to the MICS band regulation [17] or IEEE 802.15.6 standard, the maximum emission power should be below 25 μW or −16 dBm, we first use this power level in the in-body link budget analysis. Therefore, given the maximum transmit power, we can evaluate system margin when a predetermined probability of error must be guaranteed at the receiver.

The received power at the receiver front-end can be expressed using the path loss model [12], [15] under the maximum transmit power as

$$P_{r,dBW} = P_{t,dBW} - PL_{dB} \quad (15)$$

$$= P_{t,dBW} - PL_{0,dB} - 10n\log_{10}(d/d_0). \quad (16)$$

It should be noted here that the transmit and receive antenna gains were assumed as 0 dBi, and the other losses were assumed as 0 dB.

Next, under the given modulation technique of the PPM scheme with energy detection, the link signal-to-noise power ratio (SNR) or E_b/N_0 which is necessary for a receiver to achieve a specified level of reliability in terms of BER in decibel can be derived as

$$E_b/N_{0,dB} = P_{r,dBW} - 10\log_{10} f_b - N_{0,dB} \quad (17)$$

where f_b is the data rate. Thus we can define the system margin of on-body and in-body channel as M_s by

$$M_s = \frac{E_b/N_0}{[E_b/N_0]_{spec}} \quad (18)$$

where $[E_b/N_0]_{spec}$ denotes the required E_b/N_0 for obtaining a specific BER. In Eq. (18), if the link E_b/N_0 exceeds the required $[E_b/N_0]_{spec}$, which means system margin $M_s \geq 0$ dB, the wireless communication is feasible. The larger the system margin is, the more reliable and robust the communication is. Here we use BER = 10^{-2} as a predetermined probability of error threshold according to error correction theory [18], since such a BER level is able to yield error-free performance after applying appropriate forward error corrections. From the BER performance in shadow fading channel as shown in Fig. 10, we can obtain the required E_b/N_0 for BER = 10^{-2}. The corresponding values of $[E_b/N_0]_{spec}$ are 14 dB for on-body channel, and 30 dB for in-body channel, respectively. Moreover, the link budget analysis parameters are summarized in Table 3.

Table 3 Parameters for on-body and in-body link budget analysis.

Transmitter and receiver	
Frequency (MHz)	30 (On-body link) 400 (In-body link)
Transmitter output power P_t (dBm)	−10 (On-body link) −16 (In-body link)
Standard temperature T (K)	300
Receiver noise figure N_F (dB)	6
Boltzmann constant k ([J/K])	1.38×10^{-23}
Signal quality	
Bit error rate	10^{-2}
$[E_b/N_0]_{spec}$ (dB)	14 (On-body link) 30 (In-body link)

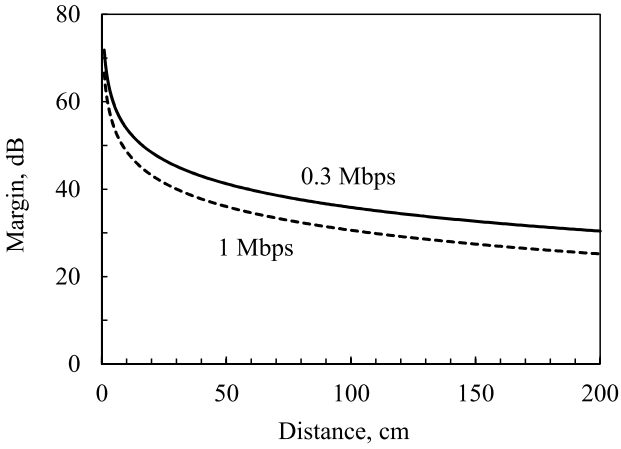

Fig. 11 Dependence of system margin on distance for on-body HBC link.

5.2 System Margin versus Link Distance

Using Eqs. (16), (17), (18), and assumed system parameters in Table 3, we can derive the system margin versus communication distance at different data rates.

Figures 11 and 12 show the dependence of system margin on link distance with a data rate of 0.3 Mbps for the on-body link and in-body link, respectively. Since we intend to look for the performance at higher data rates, we also show the results at 1 Mbps. It can be seen that in the on-body link, the system always has a margin larger than 20 dB at BER=10^{-2} within a distance of 2 m for a data rate up to 1 Mbps. This link budget result demonstrates the feasibility of the on-body to on-body HBC link for covering the entire human body area. For the in-body link, however, the system only has a margin larger than 0 dB below the distance of 9 cm at 1 Mbps. If the data rate is reduced to 0.3 Mbps, a link distance of 11 cm, which basically covers the entire range for the in-body applications, is achieved at a system margin larger than 0 dB. For example, in the typical application of sending cardiac pacemaker data to the

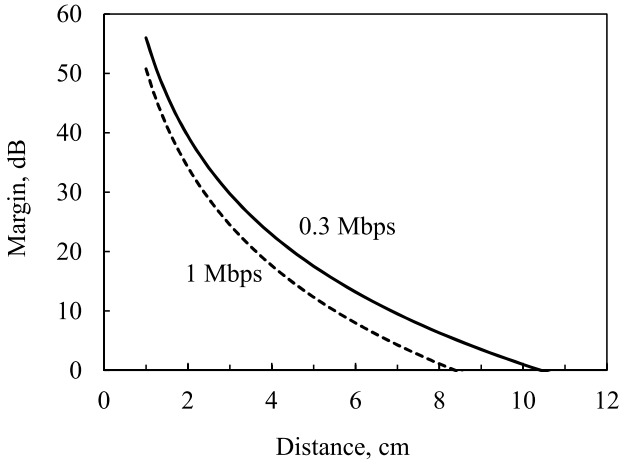

Fig. 12 Dependence of system margin on distance for in-body MICS link.

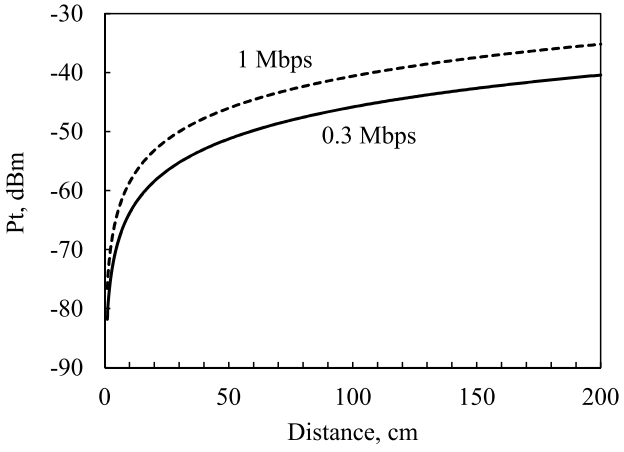

Fig. 13 Required transmit power versus link distance based on HBC on-body channel.

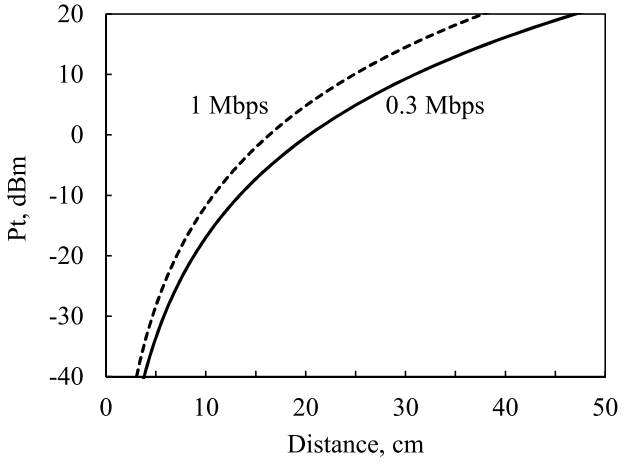

Fig. 14 Required transmit power versus link distance based on MICS in-body channel.

outside of human body, since the device is implanted at a depth of 2–3 cm, a system margin larger than 20 dB can be observed from Fig. 12 even at the data rate of 1 Mbps. For capsule endoscope application, a communication distance up to 9 cm inside the human body at 1 Mbps can also cover most of parts of the small intestine, although there is almost no margin. This link budget result shows the feasibility of the in-body to on-body MICS link for typical implant BAN applications. As a result, both the on-body and in-body link results demonstrate the feasibility of BAN applications in our dual-mode communication system.

5.3 Required Transmit Power

The analysis in the previous section was conducted to obey the regulation of the radio frequency wave emission laws. However, if it is permissible to increase the transmit power only based on biological safety considerations, the communication performance, especially in the in-body case, can be significantly improved. According to the International Commission on Non-Ionizing Radiation Protection (ICNIRP) safety guideline [19], any 10 g averaged specific absorption rate (SAR, the power absorbed per unit mass) is suggested not to exceed 2 W/kg for general public and 10 W/kg for occupational people. In this sense, 20 mW or 13 dBm may also be acceptable since it will never induce an SAR in the human tissue $>$ 2 W/kg in any 10 g tissue. As a result, it is worthwhile for us to clarify the relationship between the required transmit power and the link distance or date rate. The required transmit power can be derived from Eqs. (16) and (17) as

$$P_{t,dBW} = E_b/N_{0,dB} + N_{0,dB} + 10\log_{10} f_b + PL_{0,dB} + 10n\log_{10}(d/d_0). \quad (19)$$

Using this expression and the parameters tabulated in Tables 1 and 3, we first analyzed the maximum link distance to clarify its dependence on required transmit power at a given data rate f_b of 0.3 Mbps and 1 Mbps. Here, the E_b/N_0 is set to $[E_b/N_0]_{spec}$ to obtain a BER of 10^{-2}.

Figures 13 and 14 show the required transmit power as a function of link distance based on HBC on-body channel and MICS in-body channel. The result shown in Fig. 13 indicates that a very low transmit power is sufficient to assure an on-body to on-body HBC link. That is because even though the link distance can be as 2 m, the required transmit power will never exceed −30 dBm, which is much weaker than the level to satisfy the regulation of extremely low power radio station. By contrast, in the in-body to on-body link channel shown in Fig. 14, the feasibility of a link distance of 20 cm and 16 cm can be observed under the transmit power below 0 dBm at a data rate of 0.3 Mbps and 1 Mbps, respectively. If we furthermore increase the transmit power to 10 dBm, the link distance may extend to 30 cm and 25 cm respectively. Such a transmit power level does not cause any biological effect to the human body from the point of view of SAR restriction for general public. Moreover, a longer link distance demonstrates that the implant BAN applications may not be restricted within a small region. This has a

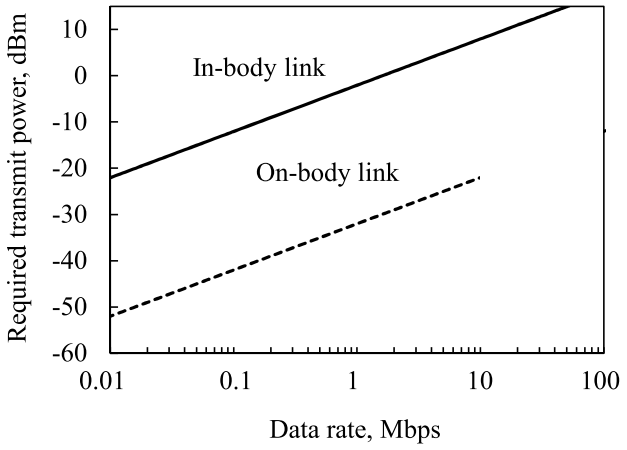

Fig. 15 Required transmit power versus data rate at distance of 1.5 m for on-body link and 15 cm for in-body link.

sufficient potential to be applied for wireless capsule endoscope at a higher data rate.

We therefore further give the relationship between the data rate and required transmit power at a desirable link distance. Here the link distance d in Eq. (19) is set to 1.5 m and 15 cm for on-body and in-body communications respectively. Since we assume a capsule endoscope application for in-body to on-body communication, the distance from small intestines to human body surface is almost always within 15 cm. Figure 15 shows the analysis result of required transmit power as a function of data rate with a fixed distance for both on-body and in-body links. This result indicates that, for on-body communication, a very low transmit power is usually sufficient for providing a high data rate up to 10 MHz. For in-body communication, a data rate of 0.3 Mbps can be realized with a transmit power below −8 dBm, and 1 Mbps below 0 dBm, respectively. If the transmit power is allowed up to 13 dBm, the data rate up to 30 Mbps can be achieved. It should be noted here that the above analysis is on the basis of SAR restriction on biological effects to the human body, not the radio frequency emission regulation. Actually, if we consider the 400 MHz band for in-body communication not as the MICS band but an extremely low power radio, the permissible electric field intensity at a distance of 3 m is 35 μV/m. In view of the significant attenuation through the in-body to on-body transmission, a transmit power larger than the prescribed −16 dBm is completely possible.

6. Conclusions

A dual-mode communication system for both on-body HBC band and in-body MICS band communications has been proposed and evaluated via computer simulations based on realistic channel model parameters. The proposed receiver uses a signal estimator to handle the dual-mode signals from on-body and in-body transmitters. Computer simulation results verified the good signal estimation performance and BER performance of the dual-mode communication system. The BER performance due to the signal estimation process was found to degrade only 1 dB and 3 dB at BER = 10^{-2} over the on-body and in-body shadow fading channel respectively, which suggests the feasibility of the dual-mode receiver structure. Moreover, the link budget analysis has been conducted based on the derived BER performances and the analysis results have demonstrated the feasibility of this dual-mode communication system. It has been found that a transmit power as low as −20 dBm is sufficient for on-body HBC link to realize a high data rate up to 10 Mbps within the entire range for HBC communications. In contrast, an in-body to on-body MICS link may achieve a data rate of 0.3 Mbps at a distance of 11 cm according to the radio frequency emission regulation. If transmit powers are allowed up to 13 dBm which still does not cause any biological effects based on the SAR consideration, very high date rates up to 30 Mbps at a link distance of 15 cm can be achieved. This suggests sufficient potential for real-time video transmission.

Our further research will improve transmit signal format and receiver structure for realization of simultaneous dual-mode transmission.

Acknowledgment

This study is supported by Grant-in-Aid for Scientific Research (Grant number 24560452).

References

[1] A.W. Astrin, H.-B. Li, and R. Kohno, "Standardization for body area networks," IEICE Trans. Commun., vol.E92-B, no.2, pp.366–372, Feb. 2009.
[2] E. Monton, J.F. Hernandez, J.M. Blasco, T. Herve, J. Micallef, I. Grech, A. Brincat, and V. Traver, "Body area network for wireless patient monitoring," IET Commun., vol.2, no.2, pp.215–222, Feb. 2008.
[3] G. Iddan, G. Meron, A. Glukhovsky, and P. Swain, "Wireless capsule endoscopy," Nature, vol.405, p.417, May 2000.
[4] M.R. Yuce and T. Dissanayake, "Easy-to-swallow wireless telemetry," IEEE Microw. Mag., pp.90–101, Sept.t 2012.
[5] J. Wang and Q. Wang, Body Area Communications, Wiley-IEEE, 2013.
[6] R. Chavez-Santiago, A. Khaleghi, I. Balasingham, and T.A. Ramstad, "Architecture of an ultra wideband wireless body area network for medical applications," 2nd International Symposium on, ISABEL 2009, pp.1–6, 2009.
[7] S. Peter and Y. Hao, eds., Antennas and Propagation for Body-Centric Wireless Communications, Artech House, Norwood, MA, 2006.
[8] A. Taparugssanagorn, A. Rabbachin, M. Hamalainen, J. Saloranta, and J. Iinatti, "A review of channel modeling for wireless body area network in wireless medical communications," Proc. 11th International Symposium on Wireless Personal Multimedia Communications, FL3–1, Sept. 2008.
[9] N. Katayama, K. Takizawa, T. Aoyagi, J. Takada, H.-B. Li, and R. Kohno, "Channel model on various frequency bands for wearable body area network," IEICE Trans. Commun., vol.E92-B, no.2, pp.418–424, Feb. 2009.
[10] R. Chavez-Santiago, K. Sayrafian-Pour, A. Khaleghi, K. Takizawa, J. Wang, I. Balasingham, and H.-B. Li, "Propagation models for IEEE 802.15.6 standardization of implant communication in body

area networks," IEEE Commun. Mag., pp.80–87, Aug. 2013.
[11] J. Wang, Y. Nishikawa, and T. Shibata, "Analysis of on-body transmission mechanism and characteristic based on an electromagnetic field approach," IEEE Trans. Microw. Theory Tech., vol.57, no.10, pp.2464–2470. Oct. 2009.
[12] J. Shi and J. Wang, "Dual-mode impulse radio ultra-wideband transmission for body area networks," IET Microwave Antennas & Propaga., vol.5, no.10, pp.1250–1255, July 2011.
[13] Y. Takagi, D. Anzai, and J. Wang, "Performance evaluation on dual-mode transceivers in wireless body area networks," Proc. 7th International Symposium on Medical Information and Communication Technology, pp.9–13, March 2013.
[14] IEEE Standard for local and metropolitan area networks–Part 15.6: Wireless Body Area Networks, Feb. 2012.
[15] D. Anzai, S. Aoyama, M. Yamanaka, and J. Wang, "Impact of spatial diversity reception on SAR reduction in implant body area networks," IEICE Trans. Commun., vol.E95–B, no.12, pp.3822–3829, Dec. 2012.
[16] A. Sani, A. Alomainy, and Y. Hao, "Numerical characterization and link budget evaluation of wireless implants considering different digital human phantoms," IEEE Trans. Microw. Theory Tech., vol.57, no.10, pp.2605–2613, Oct. 2009.
[17] H.B. Li, K.Y. Yazdandoost, and B. Zhen, "Wireless body area networks," pp.21–24, River Publisher, Feb. 2011.
[18] J.C. Bic, D. Duponteil, and J.C. Imbeaus, Elements of Digital Communication, pp.230–234, John Wiley & Sons, 1991.
[19] ICNIRP, Guidelines for limiting exposure to time-varing electric, magnetic and electromagnetic fields (up to 300 GHz), Heath Physics, vol.74, no.4, pp.494–522, 1998.

Jingjing Shi received the B.E. degree from Shenyang University of Chemical Technology, Shenyang, China, in 2007, and the M.E. and D.E. degrees from Nagoya Institute of Technology, Nagoya, Japan, in 2010 and 2013, respectively. She is currently at Nagoya Institute of Technology as a Postdoctal Research Associate. Her research interests involve biomedical communications in wireless communication networks.

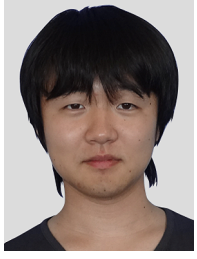

Yuki Takagi received the B.E. degree from Nagoya Institute of Technology, Aichi, Japan in 2012. He is currently pursuing the M.E. course at Nagoya Institute of Technology, engaging in the research on dual-mode transceivers in wireless body area networks.

Daisuke Anzai received the B.E., M.E. and Ph.D. degrees from Osaka City University, Osaka, Japan in 2006, 2008 and 2011, respectively. Since April 2011, he has been an Assistant Professor at the Graduate School of Engineering, Nagoya Institute of Technology, Nagoya, Japan. He has engaged in the research of biomedical communication systems and localization systems in wireless communication networks.

Jianqing Wang received the B.E. degree in electronic engineering from Beijing Institute of Technology, Beijing, China, in 1984, and the M.E. and D.E. degrees in electrical and communication engineering from Tohoku University, Sendai, Japan, in 1988 and 1991, respectively. He was a Research Associate at Tohoku University and a Senior Engineer at Sophia Systems Co., Ltd., prior to joining the Nagoya Institute of Technology, Nagoya, Japan, in 1997, where he is currently a Professor. His research interests include biomedical communications and electromagnetic compatibility.